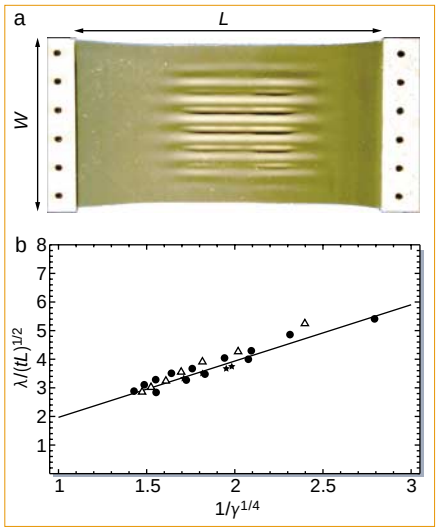

Figure 1 Wrinkles in a polyethylene sheet. **a,** Photograph of a sheet (length, L, 20 cm; width, W, 12 cm; thickness, t, 0.01 cm) under a uniaxial tensile strain, $\gamma \approx 0.1$. **b,** Plot of the dimensionless wavelength $\lambda/(tL)^{1/2}$ against $1/\gamma^{1/4}$ for various lengths of a polyethylene sheet. Lengths: circles, 25.4 cm; stars, 30.4 cm; triangles, 34.5 cm. The data span more than an order of magnitude in strain, with $\gamma \in [0.01, 0.2]$. The line corresponds to the theoretical prediction $\lambda/(tL)^{1/2} = (4\pi^2/3\gamma(1-\nu^2))^{1/4}$. For polyethylene, $\nu \approx 0.35$, so that $\lambda/(tL)^{1/2} \approx 2/\gamma^{1/4}$, which is consistent with the results of our experiments.

This non-intuitive phenomenon occurs because the clamped boundaries prevent the sheet from contracting laterally in their vicinity, setting up a local biaxial state of stress; that is, the sheet is sheared near to its boundaries. The transverse stress is tensile near the clamped boundary and compressive slightly further from it[1]. When $\gamma \approx \gamma_c$, the sheet buckles to accommodate the in-plane strain incompatibility generated by the Poisson effect. However, typically $\gamma >> \gamma_c$, so a linear theory is of little use and we must consider the geometrically nonlinear behaviour of the wrinkles.

For a sheet thus stretched, a periodic texture of parallel wrinkles of wavelength $\lambda < W$ decorates most of the sheet. The wavelength and amplitude are determined by minimizing the energy, $U = U_B + U_S$, where U_B is the energy due to bending (primarily in the transverse direction) and U_S is the energy due to stretching (along the wrinkles), subject to any geometric constraints (transverse inextensibility in this case).

If A is the amplitude of the wrinkles, then $U_B \approx Et^3(A/\lambda^2)^2LW$, whereas $U_S \approx Et\gamma(A/L)^2LW$. Transverse inextensibility implies that $(A/\lambda)^2 \approx \nu\gamma$, which quantifies the shrinkage of the sheet induced by the Poisson effect due to the imposed longitudinal strain. From this last relationship, we may derive $U \approx (Et^3/\lambda^2 + Et\gamma\lambda^2/L^2)\nu\gamma LW$. Minimizing U with respect to λ gives a scaling law for the wavelength

$$\lambda \approx (tL)^{1/2}/\gamma^{1/4} \qquad (1)$$

Substituting this relationship into the transverse-inextensibility constraint gives a scaling law for the amplitude, $A \approx (\nu tL)^{1/2}\gamma^{1/4}$. A refined calculation (E.C. and L.M., manuscript in preparation) gives the following expressions for the pre-factors: $C_\lambda = \lambda\gamma^{1/4}/(tL)^{1/2} = (4\pi^2/3(1-\nu^2))^{1/4}$, and $C_A = A/(\nu tL)^{1/2}\gamma^{1/4} = (16/3\pi^2(1-\nu^2))^{1/4}$.

To verify our results, we stretched different lengths of a polyethylene sheet of thickness ~0.01 cm and width 12 cm, by using extensional strains $\gamma \in [0.01, 0.2]$. The clamped boundary conditions were enforced by using two aluminium plates to sandwich the sheet, attached with double-sided adhesive tape to ensure that no slippage occurred. In Fig. 1b, we plot the experimental values of $\lambda/(tL)^2$ against $1/\gamma^{1/4}$, together with our theoretical prediction, which shows quantitative agreement.

Our results complement those of classical tension-field theory[2,3], which focuses on the much simpler problem of determining the locations of the wrinkles, but not their fine structure. The physics that underpins our calculation is as follows: a geometric packing constraint leads to the formation of wrinkles of intermediate wavelength because the bending resistance of the sheet penalizes short wavelengths and longitudinal stretching penalizes long wavelengths. Indeed, there is a mathematical similarity between the effect of the anisotropic tension on a curved surface and a simple elastic foundation, which allows us to generalize our results to a variety of applications (E.C. and L.M., manuscript in preparation). Moreover, inverting equation (1) yields $\gamma \approx t^2L^2/\lambda^4$, showing that wavelength is an extremely sensitive assay of strain in a wrinkled sheet.

Our results could form the basis of a quantitative wrinkling assay of thin solid films, and can potentially be applied to cell motility[4], skin biomechanics and the mechanical characterization of soft solid membranes.

E. Cerda*†, K. Ravi-Chandar‡, L. Mahadevan*

**Department of Applied Mathematics and Theoretical Physics, University of Cambridge, Cambridge CB3 9EW, UK*
e-mail: l.mahadevan@damtp.cam.ac.uk
†Departamento Fisica, Universidad de Santiago de Chile, Santiago, Chile
‡Department of Aerospace Engineering and Engineering Mechanics, University of Texas, Austin, Texas 78705, USA

1. Benthem, J. *Q. J. Mech. Appl. Math.* **16,** 413–430 (1963).
2. Wagner, H. *Z. Flugtech. Motorluftschiffart* Vol. 20, no. 8–12 (1929).
3. Mansfield, E. *Proc. XII Int. Congr. Theor. Appl. Mech.* (Springer, New York, 1968).
4. Harris, A. K., Wild, P. & Stopak, D. *Science* **208,** 177–179 (1980).

Competing financial interests: declared none.

Anthropogenic aerosols

Indirect warming effect from dispersion forcing

Anthropogenic aerosols enhance cloud reflectivity by increasing the number concentration of cloud droplets, leading to a cooling effect on climate that is referred to as the Twomey effect[1,2]. Here we show that anthropogenic aerosols exert an additional effect on cloud properties that is derived from changes in the spectral shape of the size distribution of cloud droplets in polluted air and acts to diminish this cooling. This finding could help to improve our understanding of the indirect aerosol effect and its treatment in climate modelling.

An equation commonly used for examination of the indirect aerosol effect is

$$r_e = \beta[3/(4\pi\rho)L/N]^{1/3} \qquad (1)$$

where ρ is the water density, r_e is the effective radius, L is the cloud liquid-water content and N is the number concentration of cloud droplets. The parameter β is an increasing function of the relative dispersion (ε) of the cloud droplet size distribution (ratio of the standard deviation to the mean radius), which is well described[3,4] by

$$\beta = (1 + 2\varepsilon^2)^{2/3}/(1 + \varepsilon^2)^{1/3} \qquad (2)$$

An increase (decrease) in effective radius causes a decrease (increase) in cloud reflectivity[1,2]. A prevailing assumption implicit in the evaluation of the indirect aerosol effect is that increasing aerosol loading does not alter ε or, hence, β. However, examination of data from field studies of the indirect aerosol effect shows that marine clouds classified as being polluted or having a continental origin generally have not only a larger N, but also a larger ε relative to unaffected marine clouds.

Figure 1 shows the dependence of ε and β on N. The points connected by lines represent cases identified by different investigators as evidence for the indirect effect. In each case, the points with lower N were characterized as background clouds and the higher points were characterized as similar clouds that had been perturbed by anthropogenic aerosols. Eleven of the 13 cases show an increase in ε that is concurrent with an increase in N, with negligible change to slight decreases in the other two; there is also a general increase in ε with N, as implied previously[5–7].

One explanation for the simultaneous increase in ε and N is that anthropogenic aerosols have a more complex chemical composition and a broader size distribution than marine aerosols, and that the more numerous small droplets formed in a

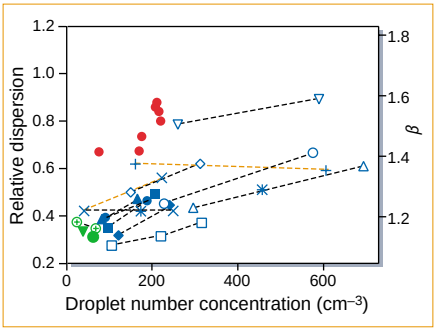

Figure 1 Relation between the relative dispersion of cloud droplet size distribution, ε, and the number concentration of cloud droplets, N. Symbols indicate programs and/or references from which the data points were derived. Connected points represent cases previously identified as evidence for an indirect aerosol effect. The parameter β is defined by equation (2). Green symbols (from ref. 8): triangle, FIRE, northeastern Pacific; crossed circles, SOCEX, Southern Ocean; filled circle, ACE1, Southern Ocean. Blue symbols: filled circles, ASTEX[8], northeastern Atlantic; diamonds, SCMS[8], Florida coast; filled triangles, Sounding[9], ASTEX; filled squares, horizontal[9], ASTEX; open inverted triangles, level 1; open upright triangles, level 2; open circles, level 3 — all from southwest of San Diego[10]; open diamonds, SCMS[11]; stars, vertical, ASTEX[12]; plus signs, horizontal, ASTEX[12]; multiplication signs, ASTEX[13]; squares, INDOEX, Indian Ocean (G. M. McFarquhar, personal communication). Red circles, MAST[6,14,15], California coast.

polluted cloud compete for water vapour and broaden the droplet size distribution compared with clean clouds that have fewer droplets and less competition.

According to equations (1) and (2), an increase in ε acts to negate the effect of increased N on effective radius and cloud reflectivity. Because this effect has been largely neglected in estimates of the indirect aerosol effect, cooling by an indirect aerosol effect is likely to have been overestimated. From the data presented in Fig. 1, we estimate that a 15% increase in N at $N = 100$ cm^{-3} causes a total forcing that ranges between -0.19 and -0.93 W m^{-2}, which corresponds to a factor that is 10–80% lower than the -1.03 W m^{-2} calculated for the Twomey effect alone[2].

The effect of the enhancement in ε is evidently large enough to be considered in assessing the indirect aerosol effect, and understanding the relation between ε and N will help to reduce the large uncertainty inherent in this effect.

Yangang Liu, Peter H. Daum
Brookhaven National Laboratory, Upton, New York 11973, USA
e-mail: lyg@bnl.gov

1. Twomey, S. *Atmos. Environ.* **8,** 1251–1256 (1974).
2. Charlson, R. J. *et al. Science* **255,** 423–430 (1992).
3. Liu, Y. & Daum, P. H. *Geophys. Res. Lett.* **27,** 1903–1906 (2000).
4. Liu, Y. & Daum, P. H. *Proc. 13th Int. Conf. On Clouds and Precipitation, Reno, USA* 586–589 (2000).
5. Martin, G. M., Johnson, D. W. & Spice, A. *J. Atmos. Sci.* **51,** 1823–1842 (1994).
6. Ackerman, A. S. *et al. J. Atmos. Sci.* **57,** 2684–2695 (2000).
7. McFarquhar, G. M. & Heymsfield, A. J. *J. Geophys. Res. D* **106,** 28675–28698 (2001).
8. Yum, S. S. & Hudson, J. G. *Atmos. Res.* **57,** 81–104 (2001).
9. Hudson, J. G. & Yum, S. S. J. *Atmos. Sci.* **54,** 2642–2654 (1997).
10. Noonkester, V. R. J. *Atmos. Sci.* **41,** 829–845 (1984).
11. Hudson, J. G. & Yum, S. S. J. *Atmos. Sci.* **58,** 915–926 (2001).
12. Garrett, T. J. & Hobbs, P. V. J. *Atmos. Sci.* **52,** 2977–2984 (1995).
13. Hudson, J. G. & Li, H. J. *Atmos. Sci.* **52,** 3031–3040 (1995).
14. Noone, K. J. *et al. J. Atmos. Sci.* **57,** 2729–2747 (2000).
15. Noone, K. J. *et al. J. Atmos. Sci.* **57,** 2748–2764 (2000).

Competing financial interests: declared none.

COMMUNICATIONS ARISING

Palaeoanthropology

Sahelanthropus or '*Sahelpithecus*'?

Beginning with *Ramapithecus*, there has been a continued search for an ape-like hominid ancestor in the Miocene Epoch. *Sahelanthropus tchadensis* is an enigmatic new Miocene species, whose characteristics are a mix of those of apes and *Homo erectus* and which has been proclaimed by Brunet *et al.* to be the earliest hominid[1]. However, we believe that features of the dentition, face and cranial base that are said to define unique links between this Toumaï specimen and the hominid clade are either not diagnostic or are consequences of biomechanical adaptations. To represent a valid clade, hominids must share unique defining features[2], and *Sahelanthropus* does not appear to have been an obligate biped.

We consider the following features that are proposed by Brunet *et al.* to constitute links with the hominid clade. First, they note that the canine is small. The canine breadth (the length is not given) is similar to the chimpanzee mean, being within the range of both chimpanzee and gorilla females and of chimpanzee males. The crown is low and the root is narrow relative to the crown, suggesting that Toumaï might have been female (canine area is a more reliable sex indicator than brow ridges); however, the postcanine teeth are all large compared with chimpanzees — as in several Miocene ape females.

The canine shows apical wear and has a thin strip of wear along the distal edge of the crown, which reaches the crown base. Although Brunet *et al.* conclude that the tooth was not used in honing, we find this difficult to reconcile with the details that they provide. Decades ago, when Miocene primate jaws with small canines and enlarged postcanine teeth were found, they were given distinct names (*Kenyapithecus* and *Ramapithecus*, for example) and were described as the earliest hominids because (it was assumed) the canine honing function had, by then, been replaced by tools (it was also assumed that they were bipeds)[3]. These specimens turned out to be female apes.

Second, the specimen has a large, continuous supraorbital torus, and the authors claim that there are other facial similarities to *Homo*. However, the facial similarities are mostly not with early hominids but with Pleistocene *Homo*, and therefore do not provide any phylogenetic information (no evidence hints that *Homo erectus* could be 6–7 million years old). There is little subnasal prognathism because the canines are small and the subnasal region is short, and the closely packed anterior dentition, crowded together because of the expanded postcanine teeth, explains the absence of diastemata. The vertical height of the impressive supraorbitals is greater than in any extant ape or australopithecine, and can only be matched in *Homo erectus* and in a few later humans.

The supraorbital size is attributed to strong sexual selection[1], which we consider unlikely. The size and form of the supraorbital structures are probably a mechanical response[4] to strain from anterior tooth loading in the region above the orbits, concentrated by the flexed frontofacial angle. The biomechanical model of the supraorbital region[5] would predict that an orthognathic face such as that of *Sahelanthropus*, combined with a low forehead, creates the potential for greater strain during anterior tooth loading than would a prognathic face with a higher forehead, as in African apes. Significant force during anterior tooth use is indicated by the expanded posterior temporalis musculature — this muscle forms a sagittal crest that meets the nuchal crest very high on the posterior vault, in a gorilla-like morphology that far exceeds the much weaker-muscled chimpanzee condition. The supraorbital torus is the bony response to strain.

Third, Brunet *et al.* infer that the intermediate thickness of the specimen's postcanine enamel is also an important link. However, thickened enamel relative to chimpanzees would be expected whatever the phylogenetic relations of *Sahelanthropus*, not only because of the other adaptations to a diet that requires powerful mastication, but also because thickened enamel is a plesiomorphic condition.

Fourth, the authors assign an anterior position to the foramen magnum on the basis of its front edge meeting the bicarotid and biporion chords, claiming that in chimpanzees the foramen magnum is posterior to these chords and that this positioning reflects their posture. STS 5, an obligate biped, does not differ from some chimpanzees by these criteria, however. Neither does this apply to the biporion chord of some chimpanzees, according to the position of the foramen magnum determined from photographs of 70 adult chimpanzee cranial bases aligned with the Frankfurt horizontal (J. Ahern, personal communication). This alignment is important in the determination, but we have no information